

# Extraction of the Parton Momentum-Fraction Dependence of Generalized Parton Distributions from Exclusive Photoproduction

Jian-Wei Qiu<sup>1,2,\*</sup> and Zhite Yu<sup>3,†</sup>

<sup>1</sup>Theory Center, Jefferson Lab, Newport News, Virginia 23606, USA

<sup>2</sup>Department of Physics, William & Mary, Williamsburg, Virginia 23187, USA

<sup>3</sup>Department of Physics and Astronomy, Michigan State University, East Lansing, Michigan 48824, USA

(Dated: March 19, 2024)

The  $x$  dependence of hadrons' generalized parton distributions (GPDs)  $\mathcal{F}(x, \xi, t)$  is the most difficult to extract from the existing known processes, while the  $\xi$  and  $t$  dependence are uniquely determined by the kinematics of the scattered hadron. We study the single diffractive hard exclusive processes for extracting GPDs in the photoproduction. We demonstrate quantitatively the enhanced sensitivity on extracting the  $x$  dependence of various GPDs from the photoproduction cross sections, as well as the asymmetries constructed from photon polarization and hadron spin that could be measured at JLab Hall D by GlueX Collaboration and future facilities.

**Introduction.**—The generalized parton distributions (GPDs),  $\mathcal{F}(x, \xi, t)$ , provide rich information on the confined spatial distributions of quarks and gluons inside a bound hadron (for reviews, see [1–4]). The Fourier transform of their  $t$  dependence at the forward limit  $\xi \rightarrow 0$  provides tomographic quark and gluon images of the hadron in its transverse plane as functions of the active parton momentum fraction  $x$  [5, 6]. The  $x$  moments of GPDs are responsible for many emergent hadronic properties such as the hadron's mass [7–10] and spin [11], as well as its internal pressure and shear force [12–14].

lision time to be much shorter than the lifetime of the  $A^*$ ) to suppress the quantum interference between the  $\mathcal{H}$  and  $\mathcal{F}$  [15, 16]. We referred to such an exclusive process for extracting GPDs as the single diffractive hard exclusive process (SDHEP). By exchanging different  $A^*$ , SDHEP can probe different GPDs,  $\mathcal{F} \rightarrow H, \tilde{H}, E, \tilde{E}, \dots$ , of different flavors [1–4]. A number of  $2 \rightarrow 3$  SDHEPs have been proposed for extracting GPDs [17–26], among which is the deeply virtual Compton scattering (DVCS) [17, 18], corresponding to  $B = C = \text{electron}$  and  $D = \gamma$ . In addition, a few  $2 \rightarrow 4$  SDHEPs have also been proposed for extracting GPDs [27–30].

Once the scattered hadron momentum  $p'$  is measured, the  $t$ ,  $\xi \equiv \Delta^+/(2P^+)$  with  $P = (p + p')/2$ , and collision energy of the hard exclusive subprocess  $(\Delta + p_2)^2$  are fully determined. For an SDHEP to be sensitive to the  $x$  dependence of GPDs, the remaining freedom of the hard subprocess  $\mathcal{H}$ , such as the  $q_T$  (or the angle) of the produced particle  $C$  or  $D$ , needs to be *entangled* with  $x$ , which is proportional to the relative momentum of the two exchanged partons [16]. For the DVCS, the exchange state  $A^*(\Delta)$  in Fig. 1 can be a virtual photon for the Bethe-Heitler process, a  $q\bar{q}$  pair for quark GPDs, and a pair of gluons for gluon GPDs, if we neglect terms further suppressed by powers of  $Q^2 = -(p_2 - q_1)^2$ . Since the relative momentum of the two exchanged partons is decoupled from external variation of  $Q^2$  at leading order, the measured DVCS cross sections probe GPDs through their “moments,” like  $\int dx \mathcal{F}(x, \xi, t)/(x - \xi)$  [16], which makes it very difficult to extract the full  $x$  dependence of GPDs [31]. Although QCD evolution of GPDs could introduce some sensitivity to the  $x$  dependence [32], the event rate drops very quickly when  $Q^2$  increases.

In this Letter, we study the sensitivity in extracting GPDs from exclusive photoproduction [16, 33, 34],

$$N(p) + \gamma(p_2) \rightarrow N'(p') + \pi(q_1) + \gamma(q_2). \quad (1)$$

The corresponding QCD factorization was justified in

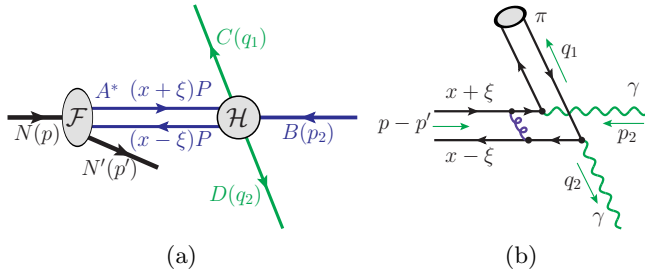


Fig. 1. (a) Sketch of  $2 \rightarrow 3$  SDHEP needed for extracting GPDs. (b) Sample diagram for the SDHEP in Eq. (1).

Experimental measurement of GPDs requires a  $2 \rightarrow 3$  exclusive process at a minimum, as sketched in Fig. 1(a), in which a hadron  $N$  of momentum  $p$  is scattered (or diffracted) to a hadron  $N'$  of momentum  $p'$  by exchanging a virtual two-parton state  $A^*$  of momentum  $\Delta \equiv p - p'$  and invariant mass  $t = \Delta^2$ , which undergoes a hard exclusive scattering with the colliding particle  $B = (\text{lepton, photon, pion})$  of momentum  $p_2$  to produce two back-to-back particles  $C(q_1)$  and  $D(q_2)$ . To ensure the separation between the hard scattering  $\mathcal{H}$  and the probed GPD  $\mathcal{F}$ , it is necessary to require the transverse momentum of the produced particles  $C$  and  $D$  to be much larger than the invariant mass of the exchange state  $A^*$ ,  $|q_{1T}| = |q_{2T}| \equiv q_T \gg \sqrt{|t|}$  (or equivalently, the hard col-

Ref. [16] by treating this process as a crossing process of the exclusive diphoton production in diffractive pion-nucleon collisions [15]. We calculate the leading-order (LO) short-distance hard parts and find that the transverse momentum (or the polar angle  $\theta$ ) of the final-state pion is clearly entangled with the relative momentum of the two exchanged partons. Variation of observed  $q_T$  can provide enhanced sensitivity to the  $x$  dependence of GPDs. With the crossing kinematics, this process provides more enhanced  $x$  sensitivity in the ERBL-region of GPDs defined to be the region where  $|x| \leq |\xi|$ , and the diphoton production in pion-nucleon scattering is more sensitive to the DGLAP-region ( $|x| > |\xi|$ ) [15]. In addition, with the well-controlled polarization of the initial-state photon beam at JLab Hall D [35] and polarized hadron targets, we introduce asymmetries of cross sections constructed from the photon beam polarization and target spin and demonstrate quantitatively the enhanced capability of extracting various GPDs and their  $x$  dependence from measurements at JLab Hall D and future facilities.

**Kinematics and observables.**—In Fig. 2, we describe the kinematics of the SDHEP in Eq. (1) in terms of two frames and two planes. The *Lab frame* is chosen to be the center-of-mass (c.m.) frame of the colliding hadron  $N(p)$  and photon  $\gamma(p_2)$  with the  $\hat{z}_{\text{lab}}$  along the momentum  $p$ , and  $\hat{x}_{\text{lab}}$  on the  $N \rightarrow N'$  diffractive plane defined by the momentum  $p$  and  $p'$ . The *SDHEP frame* is the c.m. frame of the final-state  $\pi$ - $\gamma$  pair, which is the same as the c.m. of the hard scattering subprocess, with  $\hat{z}$  along the momentum  $\Delta$  of  $A^*$ , while the initial-state photon travels along the  $-\hat{z}$  direction and  $\hat{x}$  lies on the diffractive plane. The  $\hat{z}$  and the observed  $\pi$  momentum  $q_1$  define the *scattering plane*, and the angles  $(\theta, \phi)$  define the direction of the observed  $\pi$  in the SDHEP frame. Choosing the  $(\hat{x}_{\text{lab}}, \hat{z}_{\text{lab}})$  and  $(\hat{x}, \hat{z})$  of these two frames on the same diffractive plane makes the Lorentz transformation between them simpler.

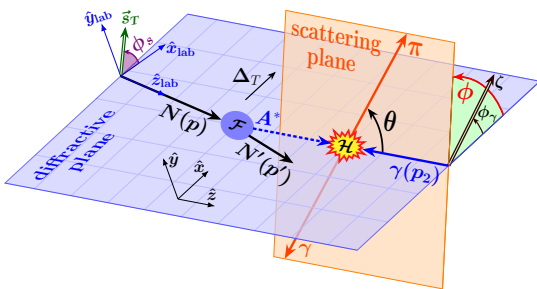


Fig. 2. Frames for the process in Eq. (1). The vectors of  $s_T$  and  $\zeta$  refer to the transverse spin and linear polarization of the colliding nucleon  $N$  and photon  $\gamma$ , respectively.

The SDHEP frame in Fig. 2 is very similar to the Breit frame for describing the lepton-hadron semi-inclusive deep inelastic scattering (SIDIS) in the Trento conven-

tion [36] if one corresponds the hadron  $N$  and  $N'$  to the colliding electron and scattered electron in SIDIS, respectively, and the diffractive plane and scattering plane to the leptonic plane and hadronic plane in SIDIS, respectively. But, unlike the highly virtual photon exchanged between the colliding lepton and hadron in SIDIS, the  $A^*$  is a “long-lived” state with a low enough virtuality.

Both the colliding photon and hadron target at JLab Hall D can be polarized longitudinally. In addition, the photon can have linear polarization  $\zeta$  and the hadron can have a transverse spin  $s_T$ , defined by the azimuthal angles,  $\phi_\gamma$  and  $\phi_s$  in the Lab frame, respectively.

Having a pion in the final state eliminates the contribution from  $A^*$  being a virtual photon due to charge parity, so that the leading contribution to the SDHEP in Eq. (1) is from channels with  $A^*$  being a collinear parton pair. The corresponding scattering amplitude can be factorized into GPDs for the hadron transition  $N \rightarrow N'$ , a distribution amplitude (DA) for the formation of the final-state pion, and perturbatively calculable coefficients [16]

$$\mathcal{M}_{N\gamma\lambda \rightarrow N'\pi\gamma\lambda'}^{[\mathcal{F}, \tilde{\mathcal{F}}]} = \sum_{f, f'} \int_{-1}^1 dx \int_0^1 dz \bar{D}_{f'/\pi}(z) \quad (2)$$

$$\times \left[ \mathcal{F}_{NN'}^f(x, \xi, t) \tilde{C}_{\lambda\lambda'}^{ff'}(x, z) + \tilde{\mathcal{F}}_{NN'}^f(x, \xi, t) C_{\lambda\lambda'}^{ff'}(x, z) \right],$$

where  $f = [q\bar{q}]$  and  $[gg]$  for quark and gluon GPDs, respectively, if  $N' = N$ , or  $f = [q\bar{q}']$  for transition GPDs with  $N \neq N'$ , and correspondingly,  $f' = [q\bar{q}]$  or  $[q\bar{q}']$  for the pion DA  $\bar{D}_{f'/\pi}$ . The hard coefficients  $C_{\lambda\lambda'}^{ff'}$  and  $\tilde{C}_{\lambda\lambda'}^{ff'}$  are helicity amplitudes for the photon scattering off a collinear on-shell parton pair  $f$  with  $\lambda$  and  $\lambda'$  denoting the photon helicities in the SDHEP frame. Under the parity invariance, they can be reduced to two helicity-conserving amplitudes ( $C_+$ ,  $\tilde{C}_+$ ) and two helicity-flipping ones ( $C_-$ ,  $\tilde{C}_-$ ). Their explicit forms are collected in Supplemental Material [37]. The correction to the factorization in Eq. (2) is suppressed by powers of  $|t|/q_T^2 \ll 1$ .

The differential cross section for the SDHEP in Eq. (1) is

$$\frac{d\sigma}{d|t| d\xi d\cos\theta d\phi} = \frac{1}{2\pi} \frac{d\sigma}{d\xi d\cos\theta} \cdot \left[ 1 + \lambda_N \lambda_\gamma A_{LL} + \zeta A_{UT} \cos 2(\phi - \phi_\gamma) + \lambda_N \zeta A_{LT} \sin 2(\phi - \phi_\gamma) \right], \quad (3)$$

where  $\lambda_N$  and  $\lambda_\gamma$  are the net helicities of the initial-state nucleon and photon, respectively. In Eq. (3), we introduced the unpolarized differential cross section,

$$\frac{d\sigma}{d|t| d\xi d\cos\theta} = \pi(\alpha_e \alpha_s)^2 \left( \frac{C_F}{N_c} \right)^2 \frac{1 - \xi^2}{\xi^2 s^3} \Sigma_{UU}, \quad (4)$$

with  $\Sigma_{UU}$  and the polarization asymmetries given by

$$\begin{aligned}\Sigma_{UU} &= |\mathcal{M}_+^{[\tilde{H}]}|^2 + |\mathcal{M}_-^{[\tilde{H}]}|^2 + |\widetilde{\mathcal{M}}_+^{[H]}|^2 + |\widetilde{\mathcal{M}}_-^{[H]}|^2, \\ A_{LL} &= 2\Sigma_{UU}^{-1} \text{Re} \left[ \mathcal{M}_+^{[\tilde{H}]} \widetilde{\mathcal{M}}_+^{[H]*} + \mathcal{M}_-^{[\tilde{H}]} \widetilde{\mathcal{M}}_-^{[H]*} \right], \\ A_{UT} &= 2\Sigma_{UU}^{-1} \text{Re} \left[ \widetilde{\mathcal{M}}_+^{[H]} \mathcal{M}_+^{[\tilde{H}]*} - \mathcal{M}_+^{[\tilde{H}]} \widetilde{\mathcal{M}}_-^{[H]*} \right], \\ A_{LT} &= 2\Sigma_{UU}^{-1} \text{Im} \left[ \mathcal{M}_+^{[\tilde{H}]} \widetilde{\mathcal{M}}_-^{[H]*} + \mathcal{M}_-^{[\tilde{H}]} \widetilde{\mathcal{M}}_+^{[H]*} \right],\end{aligned}\quad (5)$$

whose two subscripts are for hadron spin and photon polarization, respectively, with  $U$  for ‘‘unpolarized,’’  $L$  for ‘‘longitudinal polarized,’’ and  $T$  for ‘‘linearly polarized photon,’’ leaving the situation of transversely polarized hadron to a future publication. The helicity amplitudes  $\mathcal{M}_\pm^{[\tilde{H}]}$  and  $\widetilde{\mathcal{M}}_\pm^{[H]}$  in Eq. (5) are given as convolutions of GPD  $\tilde{H}$  and  $H$ , respectively, and for example,

$$\mathcal{M}_\pm^{[\tilde{H}]} = \int_{-1}^1 dx \int_0^1 dz \tilde{H}(x, \xi, t) \bar{D}(z) C_\pm(x, z; \theta) \quad (6)$$

with corresponding hard coefficients given in Supplemental Material [37]. In this Letter, we focus on contributions from quark GPDs and leave the contribution of gluon GPDs to a future publication.

**Enhanced  $x$ -sensitivity.**—While GPDs’  $t$  and  $\xi$  dependence can be directly measured, their  $x$  dependence (as well as the  $z$  dependence of DA) is only probed via convolutions as in Eq. (2). As explained in Ref. [16], the LO hard coefficient  $C$  for almost all known processes for extracting GPDs has its  $x$  dependence decoupled from the measured hard scale(s), e.g., for DVCS [17, 18],

$$C_{\text{DVCS}}^{\text{LO}}(x, \xi; x_B, Q^2) = \frac{1}{x \pm \xi \mp i\epsilon} C(x_B, Q^2). \quad (7)$$

Consequently, experimental variation of the probing scale of these processes, such as  $(x_B, Q^2)$  here, has little influence on the  $x$  convolution of GPDs. Since the unpinched  $x$  poles in Eq. (7) are only localized at  $\pm\xi$ , experimental measurements of DVCS may only constrain the diagonal values of GPDs  $\mathcal{F}(\xi, \xi, t)$  through the imaginary parts and the limited ‘‘moments,’’

$$\mathcal{F}_0(\xi, t) = \mathcal{P} \int_{-1}^1 dx \frac{\mathcal{F}(x, \xi, t)}{x - \xi}, \quad (8)$$

with  $\mathcal{P}$  indicating principle-value integration. Such lack of sensitivity to the full  $x$  dependence of GPDs is also true for other known processes, including the deeply virtual meson production (DVMP) [19, 20], photoproduction of lepton [21] or photon pair [25, 38, 39], and the exclusive Drell-Yan process [22].

Having only the moment sensitivity is far from enough to map out the  $x$  distribution of GPDs. One can easily construct null solutions to Eq. (8) that give zero to the moments, diagonal values, and forward limit [31],

at which  $(\xi, t) \rightarrow 0$  and GPDs reduce to parton distribution functions. Such solutions are termed shadow GPDs, which are invisible to processes that only possess moment-type sensitivity. Although QCD evolution of GPDs in response to the variation of the probing scale might help with this situation [40], the nature of logarithmic high-order contribution makes the improvement numerically not appreciable [31] unless one goes to a sufficiently high scale [32] where the exclusive cross section itself diminishes, making it difficult to reach the desired precision.

In contrast, the hard coefficients for the SDHEP in Eq. (1), as collected in Supplemental Material [37], have not only terms in which the  $x$  dependence is decoupled from the external hard scale  $q_T$  (or equivalently, the polar angle  $\theta$ ) of the observed pion in the SDHEP frame, like that in Eq. (7), but also terms in which the  $x$  dependence cannot be factorized as in Eq. (7) and is entangled with the observed  $q_T$  (or  $\theta$ ). More precisely, the helicity-conserving hard coefficients  $C_+$  and  $\tilde{C}_+$  contain terms proportional to the product of electric charge of quark and antiquark  $e_1 e_2$ , in which the external observable  $\theta$  is entangled with the partons’ momentum fractions  $x$  and  $z$ . Their convolutions with GPD  $H$  and  $\tilde{H}$  lead to the following type of integrals:

$$\int_{-1}^1 dx \frac{(H^+, \tilde{H}^+)(x, \xi, t)}{x - x_p(\xi, z, \theta) + i\epsilon}, \quad (9)$$

with the  $x$  pole away from  $\pm\xi$  and entangled with the externally measured  $\theta$  in the form

$$x_p(\xi, z, \theta) = \xi \cdot \left[ \frac{\cos^2(\theta/2)(1-z) - z}{\cos^2(\theta/2)(1-z) + z} \right]. \quad (10)$$

Such contribution arises from Feynman diagrams with the two photons attached to two different fermion lines, like the one in Fig. 1(b), so that the momentum flow through the short-distance gluon contains both  $x$  dependence from the GPD (and  $z$  dependence from DA) and  $q_T$  (or  $\theta$ ) dependence. This special gluon propagator is responsible for the  $x_p$  form in Eq. (10). Such entanglement provides *enhanced sensitivity* to the  $x$  dependence of GPDs from the experimentally measured  $q_T$  or  $\theta$  distribution. With  $z$  going from 0 to 1,  $x_p$  in Eq. (10) goes from  $\xi$  to  $-\xi$ , scanning through the whole ERBL region of GPDs. This is complementary to the high- $q_T$  diphoton production in single diffractive pion-nucleon scattering, which scans through the whole DGLAP region of GPDs [15].

The four helicity amplitudes  $\mathcal{M}_\pm^{[\tilde{H}]}$  and  $\widetilde{\mathcal{M}}_\pm^{[H]}$  cannot be distinguished by considering only the unpolarized differential cross section in Eq. (4), from which the two amplitudes  $\mathcal{M}_+^{[\tilde{H}]}$  and  $\widetilde{\mathcal{M}}_+^{[H]}$  with enhanced  $x$  sensitivity cannot be distinguished. Fortunately, with the capability of polarizing both the photon beam and hadron

target at JLab, various polarization asymmetries can be constructed as shown in Eq. (5). The single spin asymmetry,  $A_{UT}$ , mixes the helicity-conserving and flipping amplitudes, and then depends more on the amplitudes with enhanced  $x$  sensitivity, especially on their absolute signs. The double spin asymmetries,  $A_{LL}$  and  $A_{LT}$ , provide different combinations of the GPD  $H$  and  $\tilde{H}$ . In particular,  $A_{LT}$  is given by the imaginary parts of the amplitudes, which probe the GPD values in the ERBL region due to the special  $x$  pole at  $x_p(\xi, z, \theta)$  in Eq. (10).

The unpolarized cross section plus three asymmetries in Eq. (5) can provide good information to disentangle the GPDs  $H$  and  $\tilde{H}$ . If the hadron can also be transversely polarized, the associated asymmetry can provide new information to add constraints on the GPD  $E$  and  $\tilde{E}$ , which is beyond the scope of this Letter.

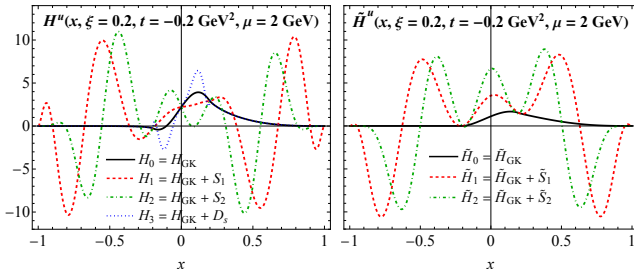


Fig. 3. Choices of the  $u$ -quark GPD models at  $t = -0.2 \text{ GeV}^2$  and  $\xi = 0.2$ , by adding shadow GPDs to the GK model.

**Numerical results.**—The CEBAF at JLab is capable of delivering intense polarized photon beam to its Hall D to study the SDHEP in Eq. (1) on various hadron targets, which can also be polarized. We evaluate the production rate and various asymmetries in Eq. (5) to demonstrate the enhanced  $x$  sensitivity on extracting GPDs. We take the Goloskokov-Kroll (GK) model [41–44] as the reference GPD for  $H$  and  $\tilde{H}$ , referred to as  $H_0$  and  $\tilde{H}_0$ , respectively. As shown in Fig. 3, we construct additional GPDs  $H_i$  and  $\tilde{H}_i$  with different  $x$  dependence from modifying the reference  $u$ -quark GPD by adding various shadow GPDs,  $S_i(x, \xi)$  or  $\tilde{S}_i(x, \xi)$ , or a shadow  $D$ -term  $D_s(x/\xi)$ , which are constructed (in Supplemental Material [37]) to give zero contribution to the GPD’s forward limit and moment in Eq. (8). We fix the pion DA to be its asymptotic form [45]. In order to focus on the  $x$  sensitivity from the  $q_T$  (or  $\theta$ ) distribution of this particular process, we neglect evolution effects of GPDs and fix both renormalization and factorization scales at 2 GeV.

In Fig. 4, we show the unpolarized differential cross section in Eq. (4) together with the various asymmetries in Eq. (5) for  $\pi^0$  production as a function of its polar angle  $\theta$  in the SDHEP frame at  $E_\gamma = 9 \text{ GeV}$ . Since the  $\cos\theta$  dependence of the hard coefficients  $C_-$  and  $\tilde{C}_-$  is multiplicative to their  $x$  or  $z$  dependence, they are not visible to the shadow GPDs. On the other hand, the  $\cos\theta$  dependence of  $C_+$  and  $\tilde{C}_+$  is entangled with their

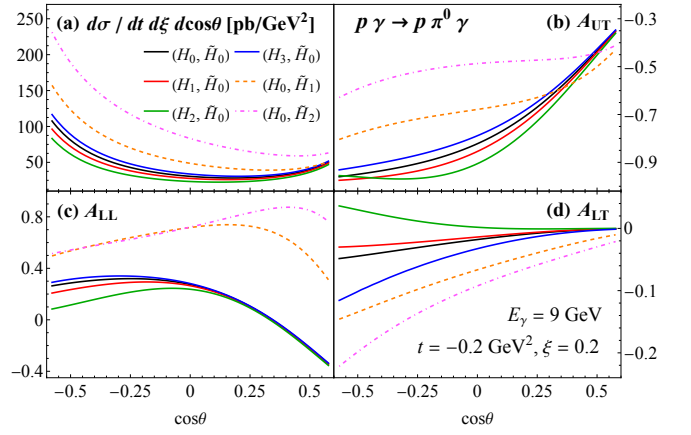


Fig. 4. Unpolarized rate (a) and polarization asymmetries (b)–(d) as functions of  $\cos\theta$  at  $(t, \xi) = (-0.2 \text{ GeV}^2, 0.2)$ , using different GPD sets as given in Fig. 3.

$x$  and  $z$  dependence, and therefore, GPDs with different  $x$  dependence lead to different rate and asymmetries. In particular, the  $A_{LT}$  is sensitive to the imaginary parts of the amplitudes, which are generated in the ERBL region, and has better sensitivity to the shadow  $D$ -term than the other three observables as shown in Fig. 4. In general, the oscillation of shadow GPDs in the DGLAP region causes a big cancellation in their contribution to the amplitudes, while the sensitivity is more positively correlated with the GPD magnitude in the ERBL region. The shadow  $\tilde{S}_i$  associated with the  $x$  dependence of the polarized GPD  $\tilde{H}$  gives bigger contribution to the amplitude  $\mathcal{M}_+^{[S]}$  than  $S_i$  to  $\tilde{\mathcal{M}}_+^{[S]}$  due to charge symmetry property, so it can be better probed.

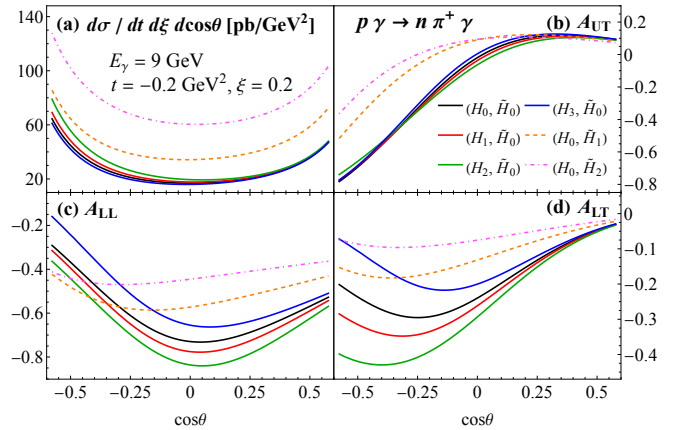


Fig. 5. Same as Fig. 4, but for the  $p\gamma \rightarrow n\pi^+\gamma$  process.

For the neutral pion production, we can eliminate terms proportional to  $(e_1 - e_2)^2$  or  $(e_1^2 - e_2^2)$  in the hard coefficients since  $e_1 = e_2$ , which effectively removes a good number of moment-type terms, giving the maxi-

imum amount of entanglement and the most sensitivity to GPDs'  $x$  dependence. In Fig. 5, we present the same study for the  $p\gamma \rightarrow n\pi^+\gamma$  process. With different flavor combination, it provides different  $x$  sensitivity. The  $n\gamma \rightarrow p\pi^-\gamma$  process gives a similar result, but with a smaller production rate. As demonstrated in Figs. 4 and 5, both the production rate and asymmetries are sizable and measurable, making the SDHEP in Eq. (1) uniquely different from DVCS and others in terms of its enhanced sensitivity for extracting the  $x$  dependence of GPDs.

**Summary and outlook.**—Extracting the full  $x$  dependence of GPDs is very important not only for probing the tomographic partonic images of hadrons, but also for predicting and understanding the emergent hadron properties in terms of various  $x$  moments of GPDs. The fact that the most known processes for extracting GPDs, including DVCS and DVMP, have only moment-type sensitivity makes it very difficult to pin down the full  $x$  dependence of GPDs and their flavor dependence due to the possibility of having an infinite number of shadow GPDs which are hardly visible to these processes.

In this Letter, we demonstrated quantitatively that the SDHEP in Eq. (1) is not only accessible by JLab Hall D but also capable of providing much enhanced sensitivity to the  $x$  dependence of GPDs, as well as the potential to probe the flavor dependence of GPDs from production rates and asymmetries involving various mesons. This is possible because this process has the entanglement of the  $x$  flow of GPDs with the externally observed hard scale [15, 16], which is a critical criterion for searching for new physical processes to help extract the  $x$  dependence of GPDs. Since multiple GPDs could contribute to the same observables through convolutions of their  $x$  dependence, extracting GPDs from data is a challenging inverse problem. A global analysis of multiple processes is necessary for extracting these nonperturbative and universal GPDs from which we can picture the spatial distribution of the probability densities to find quarks and gluons inside a bound hadron.

With the full knowledge of the  $x$ ,  $\xi$  and  $t$  dependence of GPDs, we would be able to not only address how partonic dynamics impacts the emergent hadronic properties, but also provide quantitative answers to profound questions, including what the proton radius is in terms of its transverse spatial distribution of quarks,  $r_q(x)$ , or gluons,  $r_g(x)$ , how such radii compare with its electromagnetic charge radius, and how far from the center of the proton the quarks and gluons could still be found.

**Acknowledgments.**—We thank N. Sato, J. Stevens and M. Strikman for helpful discussions and communications. This work is supported in part by the U.S. Department of Energy (DOE) Contract No. DE-AC05-06OR23177, under which Jefferson Science Associates, LLC operates Jefferson Lab. The work of Z.Y. at MSU is partially supported by the U.S. National Science Foundation under Grant No. PHY-2013791, and the fund from

the Wu-Ki Tung endowed chair in particle physics.

\* [jqiu@jlab.org](mailto:jqiu@jlab.org)

† [yuzhite@msu.edu](mailto:yuzhite@msu.edu)

- [1] K. Goeke, M. V. Polyakov, and M. Vanderhaeghen, *Prog. Part. Nucl. Phys.* **47**, 401 (2001), hep-ph/0106012.
- [2] M. Diehl, *Phys. Rept.* **388**, 41 (2003), hep-ph/0307382.
- [3] A. V. Belitsky and A. V. Radyushkin, *Phys. Rept.* **418**, 1 (2005), hep-ph/0504030.
- [4] S. Boffi and B. Pasquini, *Riv. Nuovo Cim.* **30**, 387 (2007), 0711.2625.
- [5] M. Burkardt, *Phys. Rev. D* **62**, 071503 (2000), [Erratum: *Phys.Rev.D* **66**, 119903 (2002)], hep-ph/0005108.
- [6] M. Burkardt, *Int. J. Mod. Phys. A* **18**, 173 (2003), hep-ph/0207047.
- [7] X.-D. Ji, *Phys. Rev. Lett.* **74**, 1071 (1995), hep-ph/9410274.
- [8] X.-D. Ji, *Phys. Rev. D* **52**, 271 (1995), hep-ph/9502213.
- [9] C. Lorcé, *Eur. Phys. J. C* **78**, 120 (2018), 1706.05853.
- [10] A. Metz, B. Pasquini, and S. Rodini, *Phys. Rev. D* **102**, 114042 (2020), 2006.11171.
- [11] X.-D. Ji, *Phys. Rev. Lett.* **78**, 610 (1997), hep-ph/9603249.
- [12] M. V. Polyakov, *Phys. Lett. B* **555**, 57 (2003), hep-ph/0210165.
- [13] M. V. Polyakov and P. Schweitzer, *Int. J. Mod. Phys. A* **33**, 1830025 (2018), 1805.06596.
- [14] V. D. Burkert, L. Elouadrhiri, and F. X. Girod, *Nature* **557**, 396 (2018).
- [15] J.-W. Qiu and Z. Yu, *JHEP* **08**, 103 (2022), 2205.07846.
- [16] J.-W. Qiu and Z. Yu, *Phys. Rev. D* **107**, 014007 (2023), 2210.07995.
- [17] X.-D. Ji, *Phys. Rev. D* **55**, 7114 (1997), hep-ph/9609381.
- [18] A. V. Radyushkin, *Phys. Rev. D* **56**, 5524 (1997), hep-ph/9704207.
- [19] S. J. Brodsky, L. Frankfurt, J. F. Gunion, A. H. Mueller, and M. Strikman, *Phys. Rev. D* **50**, 3134 (1994), hep-ph/9402283.
- [20] L. Frankfurt, W. Koepf, and M. Strikman, *Phys. Rev. D* **54**, 3194 (1996), hep-ph/9509311.
- [21] E. R. Berger, M. Diehl, and B. Pire, *Eur. Phys. J. C* **23**, 675 (2002), hep-ph/0110062.
- [22] E. R. Berger, M. Diehl, and B. Pire, *Phys. Lett. B* **523**, 265 (2001), hep-ph/0110080.
- [23] S. Kumano, M. Strikman, and K. Sudoh, *Phys. Rev. D* **80**, 074003 (2009), 0905.1453.
- [24] M. El Beiyad, B. Pire, M. Segond, L. Szymanowski, and S. Wallon, *Phys. Lett. B* **688**, 154 (2010), 1001.4491.
- [25] A. Pedrak, B. Pire, L. Szymanowski, and J. Wagner, *Phys. Rev. D* **96**, 074008 (2017), [Erratum: *Phys.Rev.D* **100**, 039901 (2019)], 1708.01043.
- [26] M. Siddikov and I. Schmidt, *Phys. Rev. D* **107**, 034037 (2023), 2212.14019.
- [27] M. Guidal and M. Vanderhaeghen, *Phys. Rev. Lett.* **90**, 012001 (2003), hep-ph/0208275.
- [28] A. V. Belitsky and D. Mueller, *Phys. Rev. Lett.* **90**, 022001 (2003), hep-ph/0210313.
- [29] A. V. Belitsky and D. Mueller, *Phys. Rev. D* **68**, 116005 (2003), hep-ph/0307369.
- [30] A. Pedrak, B. Pire, L. Szymanowski, and J. Wagner,

- Phys. Rev. D **101**, 114027 (2020), 2003.03263.
- [31] V. Bertone, H. Dutrieux, C. Mezrag, H. Moutarde, and P. Sznajder, Phys. Rev. D **103**, 114019 (2021), 2104.03836.
- [32] E. Moffat, A. Freese, I. Cloët, T. Donohoe, L. Gamberg, W. Melnitchouk, A. Metz, A. Prokudin, and N. Sato (2023), 2303.12006.
- [33] G. Duplančić, K. Passek-Kumerički, B. Pire, L. Szymanowski, and S. Wallon, JHEP **11**, 179 (2018), 1809.08104.
- [34] G. Duplančić, S. Nabeebaccus, K. Passek-Kumerički, B. Pire, L. Szymanowski, and S. Wallon, JHEP **03**, 241 (2023), 2212.00655.
- [35] H. Al Ghouli et al. (GlueX), Phys. Rev. C **95**, 042201 (2017), 1701.08123.
- [36] A. Bacchetta, U. D'Alesio, M. Diehl, and C. A. Miller, Phys. Rev. D **70**, 117504 (2004), hep-ph/0410050.
- [37] See Supplemental Material for the analytic forms of the hard coefficients,  $C_{\lambda\lambda'}^{ff'}$  and  $\tilde{C}_{\lambda\lambda'}^{ff'}$  in Eq. (2), the complete expressions of the helicity amplitudes,  $\mathcal{M}_{\pm}^{[H]}$  and  $\tilde{M}_{\pm}^{[H]}$  in Eq. (5), and construction of the analytic shadow GPDs in Fig. 3.
- [38] O. Grocholski, B. Pire, P. Sznajder, L. Szymanowski, and J. Wagner, Phys. Rev. D **104**, 114006 (2021), 2110.00048.
- [39] O. Grocholski, B. Pire, P. Sznajder, L. Szymanowski, and J. Wagner, Phys. Rev. D **105**, 094025 (2022), 2204.00396.
- [40] A. Freund, Phys. Lett. B **472**, 412 (2000), hep-ph/9903488.
- [41] S. V. Goloskokov and P. Kroll, Eur. Phys. J. C **42**, 281 (2005), hep-ph/0501242.
- [42] S. V. Goloskokov and P. Kroll, Eur. Phys. J. C **53**, 367 (2008), 0708.3569.
- [43] S. V. Goloskokov and P. Kroll, Eur. Phys. J. C **65**, 137 (2010), 0906.0460.
- [44] P. Kroll, H. Moutarde, and F. Sabatie, Eur. Phys. J. C **73**, 2278 (2013), 1210.6975.
- [45] G. P. Lepage and S. J. Brodsky, Phys. Rev. D **22**, 2157 (1980).

# Supplemental material for “Extraction of the Parton Momentum-Fraction Dependence of Generalized Parton Distributions from Exclusive Photoproduction”

Jian-Wei Qiu<sup>1,2,\*</sup> and Zhite Yu<sup>3,†</sup>

<sup>1</sup>Theory Center, Jefferson Lab, Newport News, Virginia 23606, USA

<sup>2</sup>Department of Physics, William & Mary, Williamsburg, Virginia 23187, USA

<sup>3</sup>Department of Physics and Astronomy, Michigan State University, East Lansing, Michigan 48824, USA

(Dated: March 19, 2024)

## A: Hard coefficients for the photon-proton scattering process

The hard coefficients  $\tilde{C}_{\lambda\lambda'}$  ( $C_{\lambda\lambda'}$ ) for the photon-proton scattering process are obtained from the diagrams in Fig. S1 by amputating the parton lines associated with the diffracted proton and produced pion, and contracting them with  $\gamma \cdot \hat{p}_1/2$  ( $\gamma_5 \gamma \cdot \hat{p}_1/2$ ) and  $\gamma_5 \gamma \cdot \hat{q}_1/2$ , respectively, for the unpolarized (longitudinally polarized) GPD, where  $\hat{p}_1 = (\Delta \cdot n) \bar{n}$

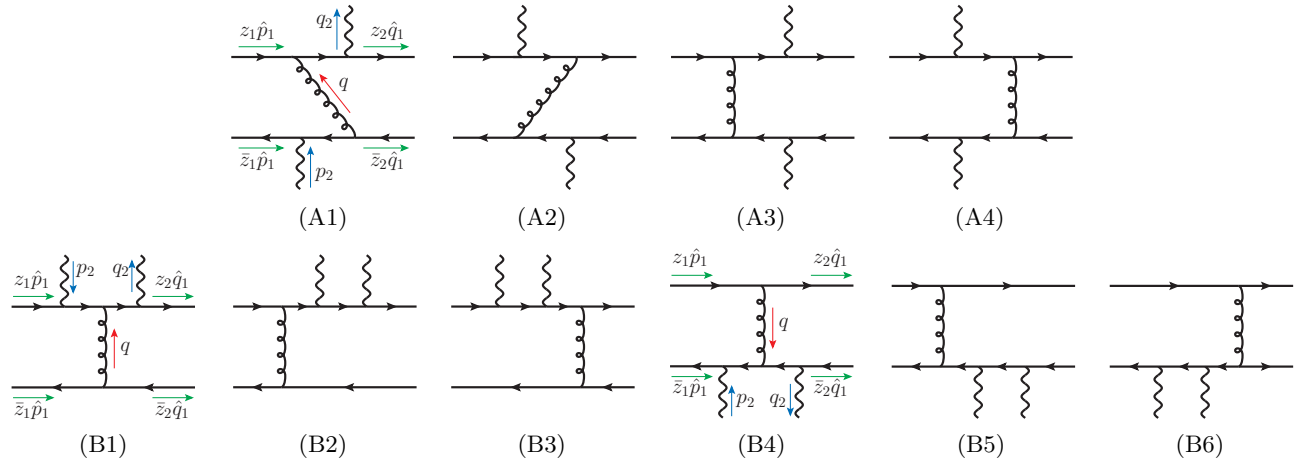


Fig. S1. Hard scattering diagrams for the photon-proton scattering into a photon-pion pair. The two incoming fermion lines on the left are from the diffracted nucleon, carrying momenta  $z_1 \hat{p}_1$  and  $\bar{z}_1 \hat{p}_1 \equiv (1 - z_1) \hat{p}_1$ , respectively. The two outgoing fermion lines on the right are to form the produced pion, carrying momenta  $z_2 \hat{q}_1$  and  $\bar{z}_2 \hat{q}_1 \equiv (1 - z_2) \hat{q}_1$ , respectively. The variables  $z_1$  and  $z_2$  are related to  $x$  and  $z$  by  $z_1 = (x + \xi)/2\xi$  and  $z_2 = z$  (see the text). Another set of diagrams are also to be included by switching the two photon lines, giving 20 diagrams in total.

with  $n = (0^+, 1^-, \mathbf{0}_T)$  and  $\bar{n} = (1^+, 0^-, \mathbf{0}_T)$ , and  $\hat{q}_1 = (q_1 \cdot w) \bar{w}$  with  $w$  and  $\bar{w}$  like  $n$  and  $\bar{n}$ , respectively, but with the corresponding  $\hat{z}$ -axis along  $\bar{q}_1$ . The helicity amplitudes are parametrized in terms of the center-of-mass energy squared  $\hat{s} = s(1 + \xi)/(2\xi)$ , the angles  $(\theta, \phi)$  of the pion in the SDHEP frame, and the parton momentum fractions  $x$  and  $z$ ,

$$\begin{aligned} C_{\pm\pm}(x, z; \hat{s}, \theta, \phi) &= \frac{\mathcal{N}}{\hat{s}} e^{\mp i\phi} C_+(x, z; \theta), & C_{\pm\mp}(x, z; \hat{s}, \theta, \phi) &= \frac{\mathcal{N}}{\hat{s}} e^{\mp i\phi} C_-(x, z; \theta), \\ \tilde{C}_{\pm\pm}(x, z; \hat{s}, \theta, \phi) &= \pm \frac{\mathcal{N}}{\hat{s}} e^{\mp i\phi} \tilde{C}_+(x, z; \theta), & \tilde{C}_{\pm\mp}(x, z; \hat{s}, \theta, \phi) &= \pm \frac{\mathcal{N}}{\hat{s}} e^{\mp i\phi} \tilde{C}_-(x, z; \theta), \end{aligned} \quad (S1)$$

where  $\mathcal{N} = 2ie^2g^2C_F/N_c$  is a normalization factor, and we have used parity symmetry to reduce the eight helicity amplitudes into four independent ones, the two helicity-conserving ones,  $C_+$  and  $\tilde{C}_+$ , and two helicity-flipping ones,  $C_-$  and  $\tilde{C}_-$ . To present these amplitudes with the charge-conjugation symmetry manifestly exhibited, we introduce the variables  $z_1 = (x + \xi)/(2\xi)$  and  $z_2 = z$ , such that when we picture the parton pair state  $A^* = [q\bar{q}']$  as a virtual meson with two valence partons of light-cone momentum fraction  $z_1$  and  $(1 - z_1)$ , respectively. Then the four independent helicity amplitudes are,

$$\begin{aligned} 2\xi C_+(\theta; x, z) &= -(e_1 - e_2)^2 \left[ \frac{1 - \cos \theta}{1 + \cos \theta} \cdot \mathcal{P} \frac{z_1 + z_2 - 2z_1z_2}{2z_1z_2(1 - z_1)(1 - z_2)} \right] + (e_1^2 - e_2^2) \left[ \frac{2}{1 - \cos \theta} \cdot \mathcal{P} \frac{z_1 - z_2}{z_1z_2(1 - z_1)(1 - z_2)} \right] \\ &+ e_1e_2 \mathcal{P} \left[ \frac{1 - \cos \theta}{z_1z_2(1 - z_1)(1 - z_2)} \cdot \frac{(z_1z_2 + (1 - z_1)(1 - z_2))(z_1(1 - z_1) + z_2(1 - z_2))}{(2(1 - z_1)(1 - z_2) - (1 + \cos \theta)z_1z_2)(2z_1z_2 - (1 + \cos \theta)(1 - z_1)(1 - z_2))} \right] \end{aligned}$$

$$\begin{aligned}
& + i\pi \left\{ (e_1 - e_2)^2 \frac{2 \cos \theta}{\sin^2 \theta} \left( \frac{\delta(1 - z_1)}{z_2} + \frac{\delta(z_1)}{1 - z_2} \right) + \frac{(e_1^2 - e_2^2)}{2} \cdot \frac{3 - \cos \theta}{1 - \cos \theta} \left( \frac{\delta(1 - z_1)}{z_2} - \frac{\delta(z_1)}{1 - z_2} \right) \right. \\
& \quad - \frac{e_1 e_2}{2} \left( \frac{1 - \cos \theta}{1 + \cos \theta} - \frac{4}{1 - \cos \theta} \right) \left( \frac{\delta(1 - z_1)}{z_2} + \frac{\delta(z_1)}{1 - z_2} \right) - \frac{e_1 e_2}{(1 + \cos \theta) z_2 (1 - z_2)} \times \\
& \quad \left. \times \left[ \left( \frac{z_1}{1 - z_2} + \frac{1 + \cos \theta}{2} \frac{1 - z_2}{z_1} \right) \delta(z_1 - \rho(z_2)) + \left( \frac{1 + \cos \theta}{2} \frac{z_1}{1 - z_2} + \frac{1 - z_2}{z_1} \right) \delta(z_1 - \tilde{\rho}(z_2)) \right] \right\}, \quad (\text{S2})
\end{aligned}$$

$$\begin{aligned}
2\xi C_-(\theta; x, z) &= -(e_1 - e_2)^2 \left[ \frac{1 - \cos \theta}{1 + \cos \theta} \cdot \mathcal{P} \frac{z_1 z_2 + (1 - z_1)(1 - z_2)}{2 z_1 z_2 (1 - z_1)(1 - z_2)} \right] \\
& - i\pi \left\{ \frac{(e_1 - e_2)^2}{1 + \cos \theta} \left( \frac{\delta(1 - z_1)}{1 - z_2} + \frac{\delta(z_1)}{z_2} \right) + \frac{e_1^2 - e_2^2}{2} \left( \frac{\delta(z_1)}{z_2} - \frac{\delta(1 - z_1)}{1 - z_2} \right) + \frac{2e_1 e_2}{1 + \cos \theta} \left( \frac{\delta(1 - z_1)}{1 - z_2} + \frac{\delta(z_1)}{z_2} \right) \right\}, \quad (\text{S3})
\end{aligned}$$

$$\begin{aligned}
2\xi \tilde{C}_+(\theta; x, z) &= -(e_1 - e_2)^2 \left[ \frac{3 + \cos \theta}{2(1 + \cos \theta)} \cdot \mathcal{P} \frac{z_1 - z_2}{z_1 z_2 (1 - z_1)(1 - z_2)} \right] \\
& + e_1 e_2 \mathcal{P} \left[ \frac{(3 + \cos \theta)}{z_1 z_2 (1 - z_1)(1 - z_2)} \cdot \frac{(z_1 - z_2)(1 - z_1 - z_2)^2}{(2(1 - z_1)(1 - z_2) - (1 + \cos \theta) z_1 z_2) (2z_1 z_2 - (1 + \cos \theta)(1 - z_1)(1 - z_2))} \right] \\
& + i\pi \left\{ \frac{2(e_1 - e_2)^2}{\sin^2 \theta} \left( \frac{\delta(z_1)}{1 - z_2} - \frac{\delta(1 - z_1)}{z_2} \right) + \frac{e_1^2 - e_2^2}{2} \frac{1 + \cos \theta}{1 - \cos \theta} \left( \frac{\delta(1 - z_1)}{z_2} + \frac{\delta(z_1)}{1 - z_2} \right) + \frac{e_1 e_2}{2} \times \right. \\
& \quad \left. \times \left[ \left( \frac{8}{\sin^2 \theta} - \frac{1 - \cos \theta}{1 + \cos \theta} \right) \left( \frac{\delta(z_1)}{1 - z_2} - \frac{\delta(1 - z_1)}{z_2} \right) - \frac{1 - \cos \theta}{1 + \cos \theta} \frac{z_1 - z_2}{z_2 (1 - z_2)} [\delta(z_1 - \rho(z_2)) + \delta(z_1 - \tilde{\rho}(z_2))] \right] \right\}, \quad (\text{S4})
\end{aligned}$$

$$\begin{aligned}
2\xi \tilde{C}_-(\theta; x, z) &= -(e_1 - e_2)^2 \left[ \frac{1 - \cos \theta}{1 + \cos \theta} \cdot \mathcal{P} \frac{(1 - z_1 - z_2)}{2 z_1 z_2 (1 - z_1)(1 - z_2)} \right] \\
& - i\pi \left\{ \frac{(e_1 - e_2)^2}{1 + \cos \theta} \left( \frac{\delta(z_1)}{z_2} - \frac{\delta(1 - z_1)}{1 - z_2} \right) + \frac{e_1^2 - e_2^2}{2} \left( \frac{\delta(z_1)}{z_2} + \frac{\delta(1 - z_1)}{1 - z_2} \right) + \frac{2e_1 e_2}{1 + \cos \theta} \left( \frac{\delta(z_1)}{z_2} - \frac{\delta(1 - z_1)}{1 - z_2} \right) \right\}, \quad (\text{S5})
\end{aligned}$$

where  $\mathcal{P}$  indicates that the hard coefficients should be understood in the sense of principle-value integration for  $z_1$  (or  $x$ ), when convoluted with the GPD and DA. We have expressed the amplitudes in the general flavor case with the two parton lines carrying electric charge  $e_1$  and  $e_2$ , with  $e_u = 2/3$  and  $e_d = -1/3$  for  $u$  and  $d$  quarks. For charged pion  $\pi^\pm$  productions, we have  $(e_1, e_2) = (e_u, e_d)$  or  $(e_d, e_u)$ , and all terms in Eqs. (S2)-(S5) contribute. For neutral pion production, however, we have  $e_1 = e_2 = e_u$  or  $e_d$ , which cancels the terms proportional to  $(e_1 - e_2)^2$  and  $(e_1^2 - e_2^2)$ .

The special gluon propagators in the type-A diagrams in Fig. S1 introduce new poles of  $z_1$  in addition to 0 and 1,

$$\rho(z_2) = \frac{(1 + \cos \theta)(1 - z_2)}{1 + \cos \theta + (1 - \cos \theta)z_2} = \frac{1 - z_2}{1 + z_2 \tan^2(\theta/2)}, \quad \tilde{\rho}(z_2) = 1 - \rho(1 - z_2), \quad (\text{S6})$$

both of which lie between 0 and 1 for  $z_2 \in [0, 1]$  and  $\theta \in (0, \pi)$ . They translate to poles of  $x$  at

$$x_p(\xi, z, \theta) = \xi [2\rho(z) - 1] = \xi \cdot \left[ \frac{\cos^2(\theta/2)(1 - z) - z}{\cos^2(\theta/2)(1 - z) + z} \right], \quad \tilde{x}_p(\xi, z, \theta) = \xi [2\tilde{\rho}(z) - 1] = -x_p(\xi, 1 - z, \theta), \quad (\text{S7})$$

which lie between  $-\xi$  and  $\xi$ .

The factorized helicity amplitudes are given by the convolution of the hard coefficients with the GPD  $H$  or  $\tilde{H}$  and  $\bar{D}(z)$ , which can be simplified by using  $\bar{D}(z) = \bar{D}(1 - z)$ . We have

$$\begin{aligned}
\mathcal{M}_+^{[\tilde{H}]} &\equiv \int_{-1}^1 dx \int_0^1 dz \tilde{H}(x, \xi, t) \bar{D}(z) C_+(x, z; \theta) \\
&= (e_1 - e_2)^2 \cdot \bar{D}_0 \cdot \left[ \frac{1 - \cos \theta}{2(1 + \cos \theta)} \cdot \tilde{H}_0^+(\xi, t) + \frac{2i\pi \cos \theta}{\sin^2 \theta} \cdot \tilde{H}^+(\xi, \xi, t) \right] \\
& \quad + (e_1^2 - e_2^2) \cdot \bar{D}_0 \cdot \left[ -\frac{2}{1 - \cos \theta} \cdot \tilde{H}_0^-(\xi, t) + \frac{i\pi}{2} \cdot \frac{3 - \cos \theta}{1 - \cos \theta} \cdot \tilde{H}^-(\xi, \xi, t) \right] \\
& \quad + e_1 e_2 \cdot \left\{ \int_0^1 \frac{dz \bar{D}(z)}{z(1 - z)} \left[ \frac{1}{2z + (1 + \cos \theta)(1 - z)} + \frac{2z + (1 + \cos \theta)(1 - z)}{2(1 + \cos \theta)} \right] \cdot \int_{-1}^1 dx \frac{\tilde{H}^+(x, \xi, t)}{x - x_p(\xi, z, \theta) + i\epsilon} \right. \\
& \quad \left. + \bar{D}_0 \cdot \left[ \frac{1 - \cos \theta}{2(1 + \cos \theta)} \cdot \tilde{H}_0^+(\xi, t) - i\pi \left( \frac{1 - \cos \theta}{2(1 + \cos \theta)} - \frac{2}{1 - \cos \theta} \right) \cdot \tilde{H}^+(\xi, \xi, t) \right] \right\}, \quad (\text{S8})
\end{aligned}$$



$$\begin{aligned}
\mathcal{M}_-^{[\tilde{H}]} &\equiv \int_{-1}^1 dx \int_0^1 dz \tilde{H}(x, \xi, t) \bar{D}(z) C_-(x, z; \theta) \\
&= (e_1 - e_2)^2 \cdot \bar{D}_0 \cdot \left[ \frac{1 - \cos \theta}{2(1 + \cos \theta)} \cdot \tilde{H}_0^+(\xi, t) - \frac{i\pi}{1 + \cos \theta} \cdot \tilde{H}^+(\xi, \xi, t) \right] \\
&\quad + (e_1^2 - e_2^2) \cdot \frac{i\pi}{2} \cdot \bar{D}_0 \cdot \tilde{H}^-(\xi, \xi, t) - e_1 e_2 \cdot \frac{2i\pi}{1 + \cos \theta} \cdot \bar{D}_0 \cdot \tilde{H}^+(\xi, \xi, t), \tag{S9}
\end{aligned}$$

$$\begin{aligned}
\tilde{\mathcal{M}}_+^{[H]} &\equiv \int_{-1}^1 dx \int_0^1 dz H(x, \xi, t) \bar{D}(z) \tilde{C}_+(x, z; \theta) \\
&= (e_1 - e_2)^2 \cdot \bar{D}_0 \cdot \left[ \frac{3 + \cos \theta}{2(1 + \cos \theta)} \cdot H_0^+(\xi, t) - \frac{2i\pi}{\sin^2 \theta} \cdot H^+(\xi, \xi, t) \right] \\
&\quad + (e_1^2 - e_2^2) \cdot \frac{i\pi}{2} \cdot \frac{1 + \cos \theta}{1 - \cos \theta} \cdot \bar{D}_0 \cdot H^-(\xi, \xi, t) \\
&\quad + e_1 e_2 \cdot \left\{ \int_0^1 \frac{dz \bar{D}(z)}{z(1-z)} \left[ \frac{1}{2z + (1 + \cos \theta)(1-z)} - \frac{2z + (1 + \cos \theta)(1-z)}{2(1 + \cos \theta)} \right] \cdot \int_{-1}^1 dx \frac{H^+(x, \xi, t)}{x - x_p(\xi, z, \theta) + i\epsilon} \right. \\
&\quad \left. + \bar{D}_0 \cdot \left[ \frac{3 + \cos \theta}{2(1 + \cos \theta)} \cdot H_0^+(\xi, t) - \frac{i\pi}{2} \left( \frac{8}{\sin^2 \theta} - \frac{1 - \cos \theta}{1 + \cos \theta} \right) H^+(\xi, \xi, t) \right] \right\}, \tag{S10}
\end{aligned}$$

$$\begin{aligned}
\tilde{\mathcal{M}}_-^{[H]} &\equiv \int_{-1}^1 dx \int_0^1 dz H(x, \xi, t) \bar{D}(z) \tilde{C}_-(x, z; \theta) \\
&= -(e_1 - e_2)^2 \cdot \bar{D}_0 \cdot \left[ \frac{1 - \cos \theta}{2(1 + \cos \theta)} H_0^+(\xi, t) - \frac{i\pi}{1 + \cos \theta} H^+(\xi, \xi, t) \right] \\
&\quad - (e_1^2 - e_2^2) \cdot \frac{i\pi}{2} \cdot \bar{D}_0 \cdot H^-(\xi, \xi, t) + e_1 e_2 \cdot \frac{2i\pi}{1 + \cos \theta} \cdot \bar{D}_0 \cdot H^+(\xi, \xi, t), \tag{S11}
\end{aligned}$$

where we have defined the charge-conjugation-even (C-even) and charge-conjugation-odd (C-odd) GPD combinations

$$H^\pm(x, \xi, t) \equiv H(x, \xi, t) \mp H(-x, \xi, t), \quad \tilde{H}^\pm(x, \xi, t) \equiv \tilde{H}(x, \xi, t) \pm \tilde{H}(-x, \xi, t), \tag{S12}$$

and the ‘‘zereth moments’’ of the DA and GPDs,

$$\bar{D}_0 \equiv \int_0^1 \frac{dz \bar{D}(z)}{z}, \quad F_0(\xi, t) \equiv \mathcal{P} \int_{-1}^1 \frac{dx F(x, \xi, t)}{x - \xi}, \tag{S13}$$

for  $F$  being  $H^\pm$  or  $\tilde{H}^\pm$ . We note that charge conjugation symmetry on the hard coefficients are reflected as the symmetry under  $(z_1, z_2) \leftrightarrow (1 - z_1, 1 - z_2)$  and  $e_1 \leftrightarrow e_2$  in Eqs. (S2)-(S5). As a result, the  $(e_1 - e_2)^2$  and  $e_1 e_2$  terms are probing the C-even GPD components, whereas the  $(e_1^2 - e_2^2)$  terms the C-odd GPD components. Furthermore, in the  $(e_1 - e_2)^2$  and  $(e_1^2 - e_2^2)$  terms, the  $\cos \theta$  dependence is decoupled from  $z_1$  and  $z_2$  dependence, which make the scattering amplitudes only sensitive to the moments and diagonal values of GPDs and vanish for shadow GPDs. In contrast, in the  $e_1 e_2$  terms, the  $\cos \theta$  dependence and the  $z_1$  and  $z_2$  dependence are entangled through  $x_p(\xi, z, \theta)$  and  $\tilde{x}_p(\xi, z, \theta)$  in Eq. (S7), which are capable of distinguishing shadow GPDs and provide enhanced sensitivity to the  $x$  dependence of GPDs.

## B: Construction of shadow GPDs

We define the (leading-order) shadow GPDs  $S(x, \xi)$  by requiring

$$S(x, -\xi) = S(x, \xi), \quad S(\pm 1, \xi) = 0, \quad S(x, 0) = 0, \quad S(\pm \xi, \xi) = 0, \quad \int_{-1}^1 dx \frac{S(x, \xi)}{x - \xi} = 0, \tag{S14}$$

and the  $(n + 1)$ -th moment of  $S(x, \xi)$  to be an even polynomial of  $\xi$  of at most  $n$ -th order,

$$\int_{-1}^1 dx x^n S(x, \xi) = \sum_{i=0,2,\dots}^n (2\xi)^i S_{n+1,i}, \tag{S15}$$

which ensures the shadow GPDs to have the same polynomiality and time reversal properties as normal GPDs, while they give null forward limits and vanishing contribution to the type of moment integral  $\int dx S(x, \xi, t)/(x - \xi + i\varepsilon)$ . Note that we have dropped the  $t$  dependence in  $S$ , which may be introduced to relax the small  $\xi$  suppression (due to  $S(x, 0) = 0$ ) in Eq. (S14), and the possible  $\xi^{n+1}$  term in Eq. (S15) which is associated with the  $D$ -term. We will construct a shadow  $D$ -term separately below. Since it is either the C-even or C-odd GPD combination [Eq. (S12)] that enters the scattering amplitude, we require  $S(x, \xi)$  to be either odd or even in  $x$ , when it is to be added to  $H$  or  $\tilde{H}$ . This has allowed us to leave out the condition  $\int_{-1}^1 dx S(x, \xi)/(x + \xi) = 0$  in Eq. (S14) from which it can be inferred. Besides, we also require the first moment of the shadow GPD to vanish since that can be constrained by the electromagnetic form factor measurements, i.e.,

$$\int_{-1}^1 dx S(x, \xi) = S_{1,0} = 0. \quad (\text{S16})$$

The conditions in Eq. (S14) lead to some general constraints on the shadow GPDs. In low energy scattering such as at JLab Hall D, the accessible  $\xi$  values are small,  $\xi \ll 1$ . The zeros at  $x = \pm\xi$  then severely constrain the shadow GPD values in the ERBL region, which can only grow up to a certain power of  $\xi$ . In this case, the integrals in Eq. (S16) and the last equation in Eq. (S14) mainly receive contributions from the DGLAP region, which must be highly suppressed. As a result, the shadow GPDs must have extra zeros in the DGLAP region, but not necessarily in the ERBL region. To construct specific models for shadow GPDs, we choose the following ansatz,

$$S(x, \xi) = K_0 \xi^2 x^a (x^2 - \xi^2) (1 - x^2)^b \cdot Q_{2n}(x, c), \quad (\text{S17})$$

where  $a \geq 0$  and  $b, n > 0$  are integers, and  $Q_{2n}(x, c) = 1 + cx^2 + \dots + q_{2n}(c)x^{2n}$  is an even  $2n$ -th order polynomial of  $x$ . This parametrization automatically satisfies the first four conditions in Eq. (S14). Since it is only a fourth order polynomial of  $\xi$ , the polynomiality condition can be readily satisfied. We have fixed the power of  $(x^2 - \xi^2)$  to be unity; a higher power further suppresses the ERBL region and leads to an even smaller impact. For given  $a$  and  $b$ , we choose  $n$  to be the minimum integer such that Eq. (S17) satisfies all the conditions in Eqs. (S14)(S15) and (S16). The single parameter  $c$  is allowed to tune the shape of shadow GPD. For any given choice, we choose the normalization  $K_0$  (independent of  $\xi$ ) such that  $\int_{-1}^1 dx S^2(x, \xi) = 2^2$  when  $\xi = 0.1$ .

We choose the GK model as the standard GPDs,  $H_0(x, \xi, t)$  and  $\tilde{H}_0(x, \xi, t)$ , and vary them by adding shadow GPDs to the  $u$  quark GPD. For the unpolarized GPD, we choose  $a = 1$ ,  $n = 3$ ,  $b = 2$  or  $6$ , and  $c = -11$  or  $-17$  for two shadow GPDs,  $S_1(x, \xi)$  and  $S_2(x, \xi)$ , to make up two new GPD models,  $H_{1,2} = H_0 + S_{1,2}$ . Similarly, for the polarized GPD, we choose  $a = 0$ ,  $n = 3$ ,  $b = 2$  or  $6$ , and  $c = -24$  or  $-40$  for two shadow GPDs,  $\tilde{S}_1(x, \xi)$  and  $\tilde{S}_2(x, \xi)$ , to get two more GPD models,  $\tilde{H}_{1,2} = \tilde{H}_0 + \tilde{S}_{1,2}$ .

For the unpolarized GPD, an additional term proportional to  $\text{mod}(n, 2)(2\xi)^{n+1}$  can exist on the right hand side of Eq. (S15), which comes from the  $D$ -term in the double distribution representation of GPD,

$$H^q(x, \xi, t) = \int_{-1}^1 d\beta \int_{-1+|\beta|}^{1-|\beta|} d\alpha \delta(x - \beta - \xi\alpha) f^q(\beta, \alpha, t) + \text{sgn}(\xi) D^q(x/\xi, t) \theta(\xi^2 - x^2), \quad (\text{S18})$$

where  $D^q(x, t)$  is an odd function of  $x$ . Also, to retain the conditions in Eq. (S14), we drop the  $t$  dependence and choose the shadow  $D$ -term  $D_s(x)$  such that

$$D_s(-x) = -D_s(x), \quad D_s(1) = 0, \quad \int_{-1}^1 dx \frac{D_s(x)}{x-1} = 0, \quad (\text{S19})$$

where the subscript ‘s’ is to remind that this  $D$  term is to be part of the shadow GPD, but not to be the requirement for the  $D$ -terms in the normal GPDs. Note that since the  $D$ -term automatically disappears in the forward limit, its magnitude does not necessarily suffer from the suppression when  $\xi$  is small. Because of the last condition in Eq. (S19), the shadow  $D$ -term cannot be probed by the dispersion relation in the DVCS data but it can modify the  $D$ -term in the gravitational form factor. We choose the ansatz for the shadow  $D$ -term

$$D_s(x) = J_0 x (1 - x^2) \cdot \left( 1 + cx^2 - \frac{7}{15}(3c + 5)x^4 \right) \theta(1 - x^2), \quad (\text{S20})$$

with  $c = 50$  and the normalization factor  $J_0$  chosen to make  $\int_{-1}^1 dx D_s^2(x) = 2^2$ . Adding this to the  $u$  quark GPD  $H_0$  gives another GPD model,  $H_3 = H_0 + D_s$ .